Reviews

Chemical Insights from EPR Spectra of Organometallic Radicals and Radical Ions

Anne L. Rieger and Philip H. Rieger*

Department of Chemistry, Brown University, Providence, Rhode Island 02912

Received August 5, 2003

A review of applications of electron paramagnetic resonance (EPR) to organometallics is given, covering about 35 years of the authors' work. The review includes applications where the conclusions are mainly a picture of electronic structure, though often knowledge of the singly occupied molecular orbital (SOMO) has implications for molecular structure. Included in the review are discussions of addition of a second phosphite ligand to [Co{$S_2C_2(CF_3)_2$}-$P(OMe)_3$] and a unique example of electronic isomerism (summarized on the cover).

1. Introduction

For most chemists, magnetic resonance means NMR spectra of liquid solutions, and with modern instrumentation a great deal of information can be extracted from such spectra. Isotropic EPR spectra are usually less informative. The isotropic spectrum of $[Mo(PMe_3)_2$-$(MeCCMe)Cp]^+$ is shown in Figure 1;[1] all you can really tell is that there are indeed two ^{31}P-containing ligands. The information content is buried in the components of the interaction matrixes and the orientations of the principal axes thereof, information only obtainable from solid-state samples. Unfortunately, eyes tend to glaze over with those statements. It is the purpose of this review to show that, with only a little effort, the *g* and *A* matrixes and the relative orientations of their principal axes can be obtained from EPR spectra of frozen solutions and that this information often leads to some very interesting insights regarding molecular electronic structure.

The interest in organometallic radicals is related to the importance of the frontier orbitals for the chemical properties of the molecule. Analysis of the EPR spectrum can characterize the singly occupied molecular orbital (SOMO). If the parent molecule was reduced to generate a radical anion, the SOMO is the LUMO of the diamagnetic parent; if the parent molecule was oxidized to generate a radical cation, the SOMO is the HOMO of the parent.

The results to be discussed here have accumulated in our laboratory or in the laboratories of collaborators over the past 22 years. Our initiation into the arcane world of interaction matrixes and principal axes came during a stint in the laboratories of Brian Robinson and Jim Simpson at the University of Otago, where a problem was encountered which required the kind of detailed understanding discussed here. The problem then at hand will be introduced in due course, but first some qualitative aspects of the theory of electron paramagnetic resonance spectroscopy need to be developed.

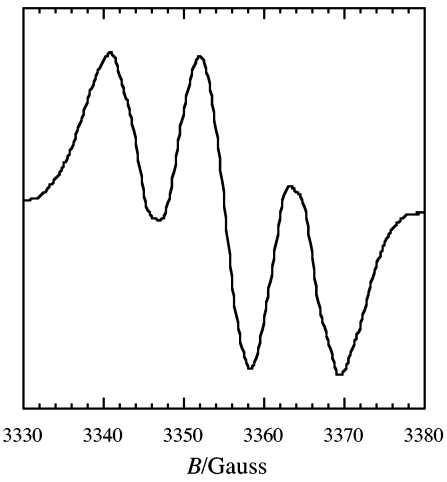

Figure 1. Isotropic EPR spectrum of $[Mo(PMe_3)_2(MeCCMe)$-$Cp]^+$ in 2/1 THF/CH_2Cl_2.

2. Theoretical Background

The major interactions which affect the EPR spectrum of a species with a single unpaired electron ($S = {}^1/_2$) are (1) the interaction of the unpaired electron with the applied magnetic field (the Zeeman effect) and (2) the interaction of the unpaired electron with magnetic nuclei in the molecule (the electron−nuclear hyperfine interaction). Both of these interactions depend on the orientation of the molecule in the applied field, and we express this orientation dependence by the matrixes $\bar{\bar{g}}$ and $\bar{\bar{A}}$, which appear in the EPR spin Hamiltonian

$$\hat{\mathbf{H}}_s = \mu_B \vec{B}\cdot\bar{\bar{g}}\cdot\vec{S} + \vec{I}\cdot\bar{\bar{A}}\cdot\vec{S}$$

where μ_B is the Bohr magneton, $\vec{B}$ is the magnetic field

(1) Adams, C. J.; Connelly, N. G.; Rieger, P. H. *J. Chem. Soc., Chem. Commun.* **2001**, 2458−2459.

10.1021/om030565e CCC: $27.50
Publication on Web 01/12/2004

strength, and $\vec{S}$ and $\vec{I}$ are the electron and nuclear angular momentum vector operators.

If the odd-electron angular momentum (and resulting magnetic moment) were due to electron spin only, the Zeeman interaction would be isotropic with $g_{xx} = g_{yy} = g_{zz} = g_e = 2.002\,32$. However, spin−orbit coupling leads to small additions of orbital angular momentum, and the interaction becomes anisotropic. There are two mechanisms for hyperfine interaction: (i) the isotropic Fermi contact interaction, proportional to the s-orbital character of the singly occupied MO (SOMO), and (ii) the inherently anisotropic electron−nuclear magnetic dipole interaction.

There are other interactions which sometimes influence EPR spectra—e.g. nuclear quadrupole coupling and, for species with more than one unpaired electron, electron−electron interactions—but here we will limit our interest to $S = {}^1/_2$ systems and consider only the g and A matrixes.

If we choose some arbitrary xyz-coordinate system to express the $\bar{\bar{g}}$ and $\bar{\bar{A}}$ matrixes, each contains off-diagonal elements, e.g.

$$\bar{\bar{g}} = \begin{pmatrix} g_{xx} & g_{xy} & g_{xz} \\ g_{yx} & g_{yy} & g_{yz} \\ g_{zx} & g_{zy} & g_{zz} \end{pmatrix}$$

$$\bar{\bar{A}} = \begin{pmatrix} A_{xx} & A_{xy} & A_{xz} \\ A_{yx} & A_{yy} & A_{yz} \\ A_{zx} & A_{zy} & A_{zz} \end{pmatrix}$$

but the matrix is diagonal when we choose a special set of coordinates, the *principal axes*:

$$\bar{\bar{g}} = \begin{pmatrix} g_{xx} & 0 & 0 \\ 0 & g_{yy} & 0 \\ 0 & 0 & g_{zz} \end{pmatrix}$$

$$\bar{\bar{A}} = \begin{pmatrix} A_{xx} & 0 & 0 \\ 0 & A_{yy} & 0 \\ 0 & 0 & A_{zz} \end{pmatrix}$$

In general, rotation about the Euler angles α, β, and γ (rotation about the z axis, the new y axis, and the new z axis, respectively) converts from the xyz coordinate system to the XYZ system. If both matrixes can be diagonalized in a single coordinate system (not necessarily an obvious molecular coordinate system), we say that the principal axes are coincident. If not, we describe the relationship between the g and A matrix principal axes by the Euler angles, rotation about which is required to convert the g matrix axes to the A matrix axes. It is in that sense that Euler angles will be referred to in this review.

In principle, the components of the g and A matrixes can be computed, given an LCAO description of the frontier molecular orbitals.[2] The g matrix components are given by

$$g_{ii} = g_e\delta_{ij} + 2\zeta\sum_{m\neq 0}\frac{\langle m|\hat{\boldsymbol{I}}_i|0\rangle\langle m|\hat{\boldsymbol{I}}_j|0\rangle}{E_0 - E_m}$$

where ζ is the spin−orbit coupling parameter for the metal in question, $|0\rangle$ is the SOMO with energy E_0, the sum is over the other molecular orbitals, $|m\rangle$ with energies E_m, i and j correspond to x, y, or z, and $\hat{\boldsymbol{I}}_x$, for example, is the x-component orbital angular momentum operator. The A matrix components are given by

$$A_{ij} = \langle A\rangle\delta_{ij} + \frac{2}{7}Pl_{ij}$$

where $\langle A\rangle$ is the isotropic hyperfine coupling, $P = g_e g_N \mu_B \mu_N \langle r^{-3}\rangle$ is usually computed from Hartree−Fock atomic orbitals,[3] and

$$l_{xx} = -c_{z^2}{}^2 - 2c_{yz}{}^2 + c_{xz}{}^2 + c_{z^2-y^2}{}^2 + c_{xy}{}^2 - 2\sqrt{3}c_{z^2}c_{x^2-y^2}$$

$$l_{yy} = -c_{z^2}{}^2 + c_{yz}{}^2 - 2c_{xz}{}^2 + c_{x^2-y^2}{}^2 + c_{xy}{}^2 - 2\sqrt{3}c_{z^2}c_{x^2-y^2}$$

$$l_{zz} = 2c_{z^2}{}^2 + c_{yz}{}^2 + c_{xz}{}^2 - c_{x^2-y^2}{}^2 + 2c_{xy}{}^2$$

$$l_{xy} = -2\sqrt{3}c_{z^2}c_{xy} + 3c_{yz}c_{xz}$$

$$l_{yz} = \sqrt{3}c_{z^2}c_{yz} + 3c_{xz}c_{xy} - 3c_{yz}c_{x^2-y^2}{}^2$$

$$l_{xz} = \sqrt{3}c_{z^2}c_{xz} + 3c_{yz}c_{xy} + 3c_{xz}c_{x^2-y^2}$$

where c_{xz}, for example, is the LCAO coefficient of d_{xz} in the SOMO.

It has long been known[4] that the principal axes of the g matrix must correspond to molecular symmetry axes or normals to reflection planes. Thus, for a molecule with C_{2v} symmetry (or higher), the molecular and g matrix axes are coincident. For a nucleus lying on a symmetry axis or in a reflection plane, the hyperfine principal axes must correspond to the rotation axis or the normal to the reflection plane. Thus, for a metal complex with C_{2v} or higher symmetry, the principal axes of the g matrix and the metal A matrix must be coincident, but ligand A matrixes in general are required to share at most one principal axis with the g matrix.

For many years, conventional wisdom in EPR spectroscopy held that the orientations of g and A principal axes could only be determined by measuring spectra of a dilute single crystal as a function of orientation in the external magnetic field. This is true in the sense that information on orientations in the *molecular* coordinate system is usually inaccessible from powder or frozen-solution spectra, but the relative orientation of the g and A axes does have an effect on powder spectra. To see this, consider the EPR spectrum of a frozen solution of an $S = {}^1/_2$ species with an $I = {}^5/_2$ nucleus where $\alpha = \gamma = 0$. To first order in perturbation theory,[5] the field positions of EPR absorptions are given by

$$B = \frac{h\nu}{g\mu_B} - \frac{Km}{g\mu_B}$$

where

$$g^2 = (g_x^2\cos^2\varphi + g_y^2\sin^2\varphi)\sin^2\theta + g_z^2\cos^2\theta$$

(2) Rieger, P. H. In *Organometallic Radical Processes*; Trogler, W. C., Ed,; Elsevier: Amsterdam, 1990.
(3) Morton, J. R.; Preston, K. F. *J. Magn. Reson.* **1978**, *30*, 577.
(4) Kneubühl, F. K. *Phys. Kondens. Mater.* **1963**, *1*, 410; **1965**, *4*, 50.
(5) In general, second-order perturbation theory corrections are also required; see: Rieger, P. H. *J. Magn. Reson.* **1982**, *50*, 485.

$$K^2 = \frac{A_x^2}{g^2}(g_x \sin\theta\cos\varphi\cos\beta + g_z\cos\theta\sin\beta)^2 + \frac{A_y^2}{g^2}(g_y\sin\theta\sin\varphi)^2 + \frac{A_z^2}{g^2}(-g_x\sin\theta\cos\varphi\sin\beta + g_z\cos\theta\cos\beta)^2$$

Using the parameters $g_x = 2.048$, $g_y = 2.105$, $g_z = 1.984$, $A_x = 20.0$, $A_y = 12.4$, $A_z = 146.1$ ($\times 10^{-4}$ cm^{-1}), and $\beta = 19.6°$—which correspond to the spectrum of [Mn(CO)(CN)(dppm)$_2$]$^+$ (see below)—the resonant field B is plotted as a function of θ and φ for $m = {}^5/_2$ in Figure 2a. The corresponding absorption and first-derivative spectra are shown in Figure 2b. Note that the minimum and maximum resonant fields (3000 and 3270 G in this case) correspond to positive- and negative-going peaks in the derivative spectrum; the baseline-crossing feature of the derivative spectrum corresponds to the most probable resonant field, usually a saddle point (a minimum with respect to one angle, a maximum with respect to the other) on the B vs θ, φ surface.

Now consider features which correspond to orientations in the xz plane ($\varphi = 0°$). Plots of g and K vs θ are shown in Figure 3a, and B is shown as a function of θ for $m = \pm{}^5/_2, \pm{}^3/_2, \pm{}^1/_2$ in Figure 3b. Figure 3c shows the field minima and maxima (for orientations in the xz plane) which would correspond to the observed features in a first-derivative powder spectrum. Note that the spacings vary. This kind of behavior is typical of noncoincident principal axes, and an analysis of the variation in spacing can be used to determine the Euler angles between two sets of principal axes.[6]

3. Two Metal Complexes Expected To Have Higher Symmetry

As the first two examples of chemically interesting insights derived from EPR matrixes, we consider two transition-metal complexes which appeared to be of C_{2v} symmetry. With the metal at the center of symmetry, it would seem that the g and A matrix principal axes must be coincident.

A three-way collaboration with groups at the University of Bristol and the University of Oviedo[7] resulted in EPR spectra of a series of low-spin Mn(II) complexes of the type [Mn(CO)(CN)(LL)$_2$]$^+$, where LL = bis(diphenylphosphino)ethane (dppe) or bis(diphenylphosphino)methane (dppm).

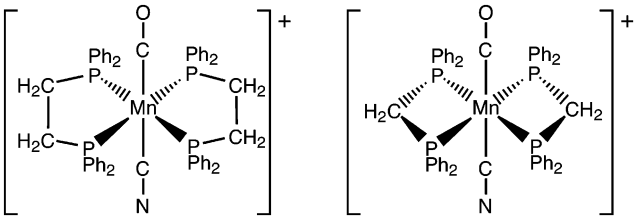

On first examination, the spectrum of the dppe derivative appeared to be a straightforward example of a highly symmetric low-spin d^5 complex. The dppm derivative, on the other hand, showed a significant variation in the spacing of minimum and maximum features; see Figures 3 and 4. Careful reexamination of the dppe spectrum revealed a much smaller noncoincidence there as well.

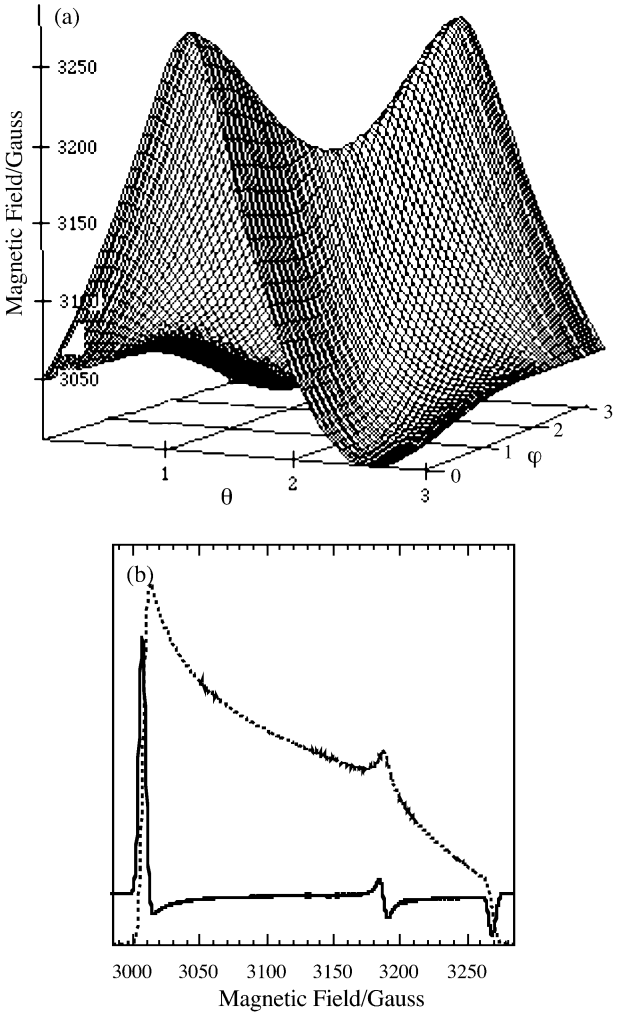

Figure 2. (a) Angular dependence of the resonant field for $m = {}^5/_2$. (b) Absorption and first-derivative spectra corresponding to (a).

Suppose that, for some reason, the molecular symmetry in these complexes is reduced to C_s with σ_{xz} as the sole remaining symmetry element. In the presumed C_{2v} symmetry, qualitative MO arguments suggest that the metal contribution to the SOMO is $d_{x^2-y^2}$, but in the reduced symmetry, d_{xz} (or d_{z^2}) could also participate (note that xz and yz are planes of symmetry so that x and y are not bond axes). Suppose then that the SOMO and the top two doubly occupied MO's can be written

$$|\mathrm{SOMO}\rangle = a_1|x^2 - y^2\rangle + a_2|\mathrm{xz}\rangle + \ldots$$

$$|\mathrm{HOMO}\rangle_1 = b|yz\rangle + \ldots$$

$$|\mathrm{HOMO}\rangle_2 = c_1|xz\rangle + c_2|x^2 - y^2\rangle + \ldots$$

Taking just these three MO's into account, the g matrix components are

(6) DeGray, J. A.; Rieger, P. H. *Bull. Magn. Reson.* **1987**, *8*, 95.
(7) Carriedo, G. A.; Connelly, N. G.; Perez-Carreno, E.; Orpen, A. G.; Rieger, A. L.; Rieger, P. H.; Riera, V.; Rosair, G. M. *J. Chem. Soc., Dalton Trans.* **1993**, 3103.

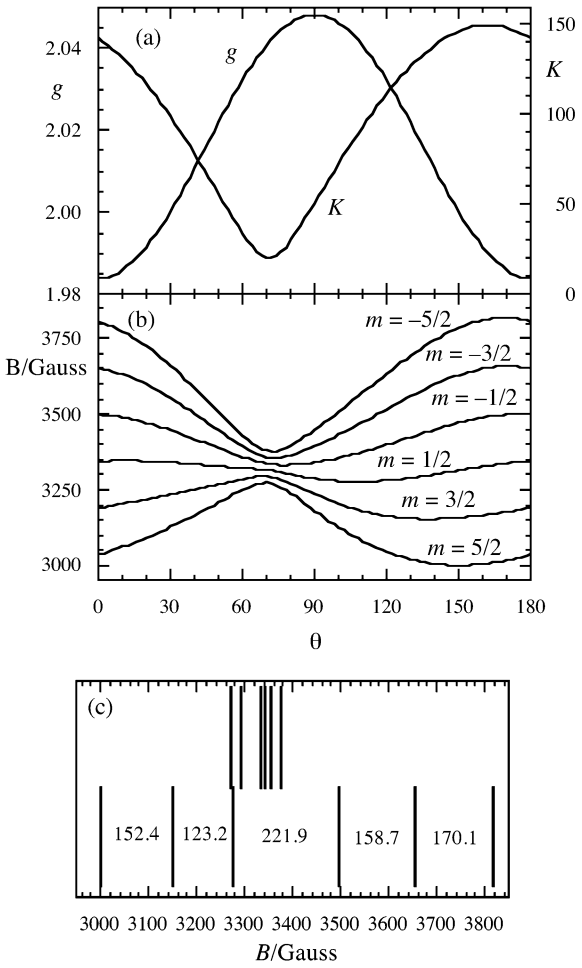

Figure 3. (a) g and K as functions of θ for $g_x = 2.048$, $g_z = 1.984$, $A_x = 20.0 \times 10^{-4}$ cm^{-1}, $A_z = 146.1 \times 10^{-4}$ cm^{-1}, and $\beta = 19.6°$. (b) Resonant fields for $m = \pm^5/_2, \pm^3/_2, \pm^1/_2$. (c) Resonant field minima and maxima.

$$g_{xx} = g_e + \frac{\zeta}{\Delta_1}(a_1 b)^2$$

$$g_{yy} = g_e + \frac{\zeta}{\Delta_2}(a_1 c_1 - a_2 c_2)^2$$

$$g_{zz} = g_e + \frac{\zeta}{\Delta_1}(a_2 b)^2$$

$$g_{xz} = -\frac{\zeta}{\Delta_1}(a_1 b)(a_2 b)$$

The g matrix is diagonalized by rotation about y by the angle β_g to give

$$g_{xx} = g_e + \frac{\zeta b^2}{\Delta_1}(a_1^2 + a_2^2)^2$$

$$g_{zz} = g_e$$

$$\tan 2\beta_g = -\frac{2a_1 a_2}{a_1^2 + a_2^2} \approx -\frac{2a_2}{a_1}$$

The hyperfine matrix components are

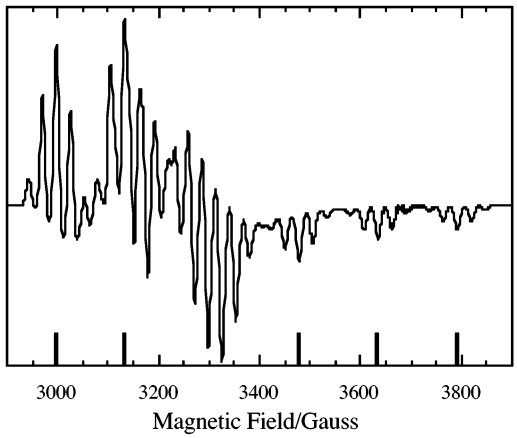

Figure 4. EPR spectrum of $[Mn(CO)(CN)(dppm)_2]^+$ in $CH_2Cl_2/C_2H_4Cl_2$ at 90 K.

$$A_{xx} = \langle A \rangle + \frac{2}{7}P(a_1^2 + a_2^2)$$

$$A_{xx} = \langle A \rangle + \frac{2}{7}P(a_1^2 + a_2^2)$$

$$A_{xx} = \langle A \rangle + \frac{2}{7}P(-2a_1^2 + a_2^2)$$

$$A_{xx} = \frac{6}{7}P a_1 a_2$$

The A matrix can also be diagonalized by rotation about y through angle β_A:

$$A_{xx} \approx \langle A \rangle + \frac{2}{7}P\left(a_1^2 + \frac{5}{2}a_2^2\right)$$

$$A_{zz} \approx \langle A \rangle - \frac{4}{7}P\left(a_1^2 + \frac{1}{4}a_2^2\right)$$

$$\tan 2\beta_A = \frac{2a_2}{a_1}$$

Note that the g and A x and z axes are rotated in opposite directions from the molecular axes so that the noncoincidence effect is magnified in the EPR spectrum:

$$\tan \beta_{obs} = \tan(\beta_A - \beta_g) = \tan 2\beta_A = \frac{2a_2}{a_1}$$

The observed principal axis noncoincidences, $\beta = 19.6°$ (dppm) and 4.6° (dppe), thus reflect the incorporation of small amounts of d_{xz} character into the SOMO's. From the measured angles, we have $a_2/a_1 = 0.18$ for the dppm complex and 0.040 for the dppe complex. Another way of describing this is to say that the $d_{x^2-y^2}$ orbital is rotated by 19.6 or 4.6° about the y axis. Once we have stated the problem in that way, it does not take long to discover the cause! In the hypothetical C_{2v} complex, there would be a strong antibonding interaction between the $d_{x^2-y^2}$ orbital and the CH_2 groups of the dppm ligands and a weaker interaction between this orbital and the CH_2CH_2 bridges of the dppe ligands. This interpretation was immediately reinforced when the X-ray structures of the Mn(I) and Mn(II) dppm derivatives were obtained (see Figure 5). The structure of the

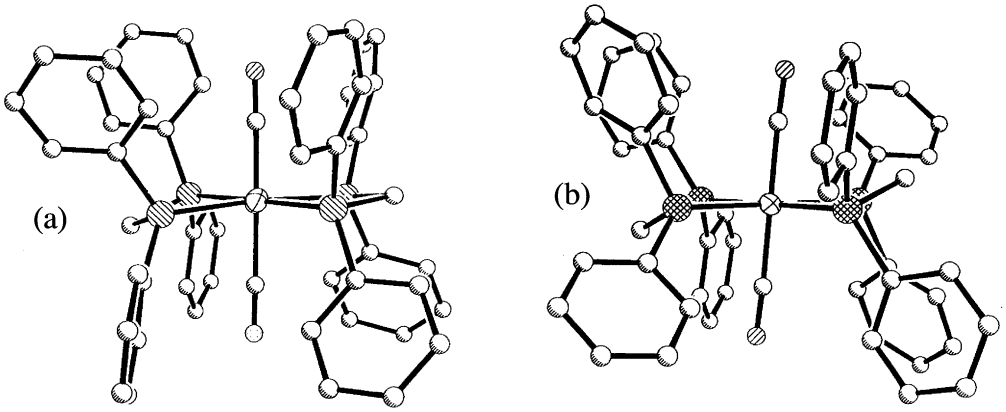

Figure 5. X-ray structures of (a) $[Mn(CO)(CN)(dppm)_2]^+$ and (b) $[Mn(CO)(CN)(dppm)_2]$.

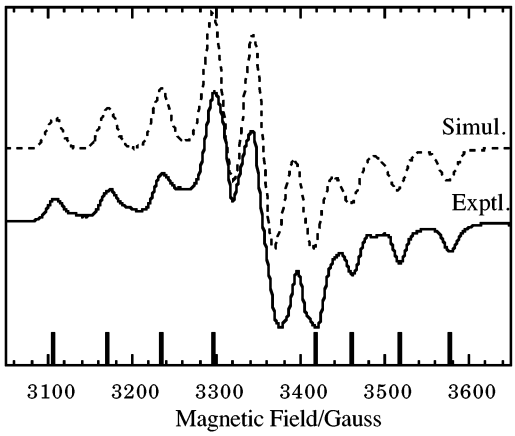

Figure 6. EPR spectrum of $[Co(S_2C_2Ph_2)_2PPh_3]$ in CH_2Cl_2/$C_2H_4Cl_2$ at 110 K.

Mn(II) derivative shows the CH_2 groups tilted up on one side of the complex and down on the other in just the way expected, given the hybridization of the SOMO. With two electrons in that orbital, the antibonding interaction is stronger, of course, and thus it is not surprising to find that the tilt of the CH_2 groups is even greater in the Mn(I) complex.

4. Cobalt Dithiolene Complexes

During the heyday of dithiolene chemistry (the mid-1960s through the early 1970s), many cobalt complexes were prepared such as $[Co(S_2C_2Ph_2)_2PPh_3]$.

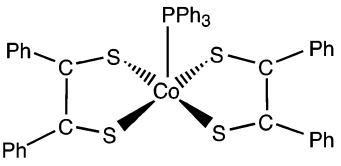

Since these are paramagnetic with a single unpaired electron, EPR spectra were usually reported, and most of them resembled that shown in Figure 6.[8] This spectrum shows unusually clear evidence for the non-coincidence of the g and A matrix principal axes. The key point is that either there are nine "parallel" hyperfine features ($I = {}^7/_2$ for ^{59}Co, so that eight hyperfine lines are expected) or there is a large gap between the fourth and fifth features. The spectrum can be interpreted in terms of a nonzero angle α between the g_x and A_x axes. A selection of data for other Co dithiolenes with other axial ligands is given in Table 2. It is clear that α increases with the steric bulk of the dithiolene R group and to some extent with the size of the axial ligand L. This interpretation has been verified by several X-ray crystal structure determinations.[7,9] As it happens, there were no X-ray structures determined for cobalt dithiolene complexes in the 1960s or 1970s, but structures were determined for several iron complexes.[10] In every case the iron complexes had virtually ideal square-pyramidal structures. The reason for the difference is not difficult to find. The EPR parameters also can be used to estimate the Co 3d character of the SOMO: 25−30% in the complexes studied. The remaining contributions almost certainly come from the S and C atoms of the dithiolene rings and, as shown in Figure 7, the SOMO is best described as a π^* orbital. Thus, the extra Co electron has the effect of making the dithiolene rings much less rigid, permitting distortions in response to steric strain.

Table 1. EPR Parameters for $[Mn(LL)_2(CO)(CN)]^+$ in $CH_2Cl_2/C_2H_4Cl_2$ at 90 K[a]

LL	g	A^{Mn}	A^P	β
dppm	2.048, 2.105, 1.984	20.0, 12.4, 146.1	25.7	19.6 ± 0.5
dppe	2.048, 2.086, 2.004	19.8, 11.0, 144.0	24.2	4.6 ± 0.9

[a] A in units of 10^{-4} cm^{-1} and β in units of deg.

In the course of our study of Co dithiolene complexes, we observed that frozen toluene solutions of $[Co\{S_2C_2(CF_3)_2\}_2P(OMe)_3]$ containing a small excess of free $P(OMe)_3$ gave temperature-dependent spectra in the 120−160 K range.[11] A detailed study of this phenomenon showed that it resulted from formation of a six-coordinate complex:

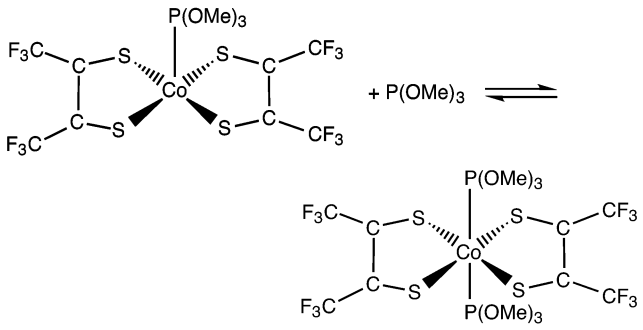

(8) Carpenter, G. B.; Clark, G. S.; Rieger, A. L.; Rieger, P. H.; Sweigart, D. A. *J. Chem. Soc., Dalton Trans.* **1994**, 2903.

Table 2. EPR Parameters for $Co(S_2C_2R_2)_2L$ for EPR Spectra in $CH_2Cl_2/C_2H_4Cl_2$ at 110 K

	R								
	CN	CF_3	CF_3	CF_3	Ph	Ph	4-MePh	4-MePh	4-MeOPh
L	PEt_3	$P(OPh)_3$	$P(OMe)_3$	PPh_3	$P(OPh)_3$	PPh_3	PEt_3	PPh_3	PPh_3
α (deg)	2 ± 2	11 ± 5	14 ± 4	16 ± 1	11 ± 5	24 ± 1	10 ± 2	24 ± 1	31 ± 2

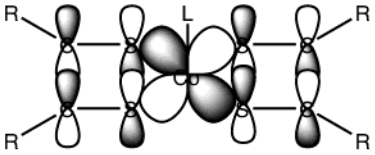

Figure 7. Schematic representation of the SOMO in $[Co(S_2C_2R_2)_2L]$.

It proved possible to determine the equilibrium constant for this process as a function of temperature, and this experiment led to $\Delta H° = -10$ kJ mol^{-1} and $\Delta S° = -68$ J mol^{-1} K^{-1}. With such a weak bond, it is not surprising that six-coordinate complexes had not been observed earlier. Of course, we cannot expect transport in frozen toluene; thus, we are really looking at a process in which $P(OMe)_3$, attracted by dipole−dipole interaction, reversibly forms a chemical bond to Co, an "outer sphere/inner sphere" equilibrium in classical inorganic terminology:

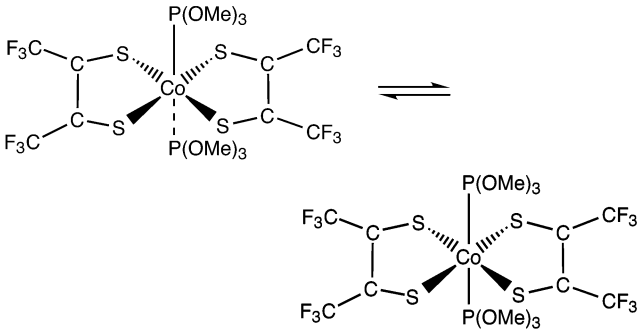

The scope of this process is quite limited. To show observable spectral changes in the 120−160 K range, we require the electron-withdrawing CF_3 groups and alkyl phosphites or phosphonites. Replacing $P(OMe)_3$ by $P(OPh)_3$ or PMe_3 or replacing CF_3 by Ph turns off the observable phenomenon.

5. "Piano-Stool" Complexes of Mn(II) and Cr(I)

Complexes such as $[(C_5H_5)Mn(CO)(PPh_3)_2]^+$ [12] can have at most a plane of symmetry so that the *g* and *A* matrix principal axes in that plane need not be coincident, and indeed they are not. EPR spectra lead to measures of the principal axis noncoincidence, which, in turn, gives information regarding the composition of the singly occupied MO and the reason for variations in SOMO composition.

EPR spectra of a variety of complexes of the type $[(\eta^5\text{-}C_5H_5)Mn(CO)L_2]^+$ and $[(\eta^5\text{-}6\text{-}exo\text{-}PhC_6H_6)Mn(CO)L_2]^+$ provide particularly dramatic examples of the effects of

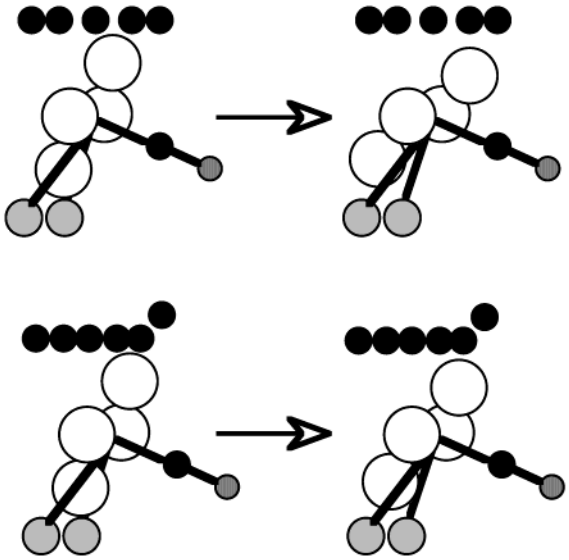

Figure 8. Schematic drawings showing relief of the antibonding interaction of the metal $d_{x^2-y^2}$ orbital with the dienyl g ring through rotation about the *y* axis by $\beta_A = 15°$ for C_6 and 35° for C_5.

principal axis noncoincidence with the Euler angle β ranging from 21° (6-*exo*PhC_6H_6) to 76° (C_5H_5).

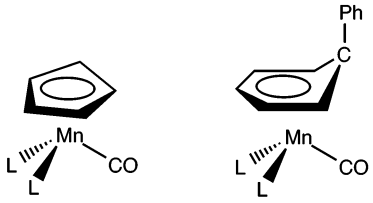

The EPR parameters lead to a description of the SOMO as an orbital with shape similar to $d_{x^2-y^2}$, but with the "x^2" lobes variably oriented in the *xz* plane, as shown in Figure 8. The variation in β is due primarily to the avoidance of antibonding interactions with the "seat" of the "piano stool" (a close analogy with the Mn(II) dppm and dppe complexes discussed above). Antibonding avoidance is easier when the SOMO lobe can fit into the slot left when one carbon of the seat is tilted upward.

Since ^{53}Cr hyperfine structure is not usually observed in frozen-solution EPR spectra of Cr(I) complexes (^{53}Cr is only 9.5% abundant), we did not expect to get any information on the orientation of the *g* matrix axes for $[(C_5Ph_5)Cr(CO)(PMe_3)_2]$.[13]

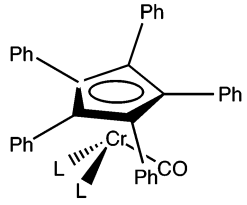

However, in this case, we were lucky. Spectra of the

(9) Carpenter, G. B.; Nochomovitz, Y. D.; Rieger, A. L.; Rieger, P. H.; Wang, H. To be submitted for publication.
(10) See literature citations in ref 7.
(11) Nochomovitz, Y. D.; Rieger, A. L.; Rieger, P. H.; Roper, B. J. *J. Chem. Soc., Dalton Trans.* **1996**, 3503.
(12) Pike, R. D.; A. L. Rieger, A. L. Rieger, P. H. *J. Chem. Soc., Faraday Trans. 1* **1989**, *85*, 3513.

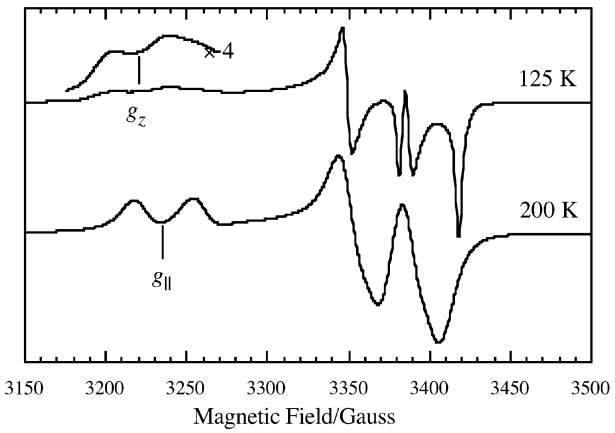

Figure 9. EPR spectra of $[(C_5Ph_5)Cr(CO)_2PMe_3]$ in toluene.

Cr(I) piano-stool complex in toluene solution are shown in Figure 9 at 125 and 200 K. The frozen-solution spectrum shows the expected three *g* components, each of which is a triplet due to ^{31}P coupling. The low-field feature is unexpectedly broad, but that is another story.[14] The interesting story here is the spectrum at 200 K, where toluene is a liquid. Because the viscosity at 200 K is high, the bulky C_5Ph_5 ligand is still essentially stationary on the EPR time scale, but the "legs" of the piano stool, $Cr(CO)_2PMe_3$, are freely rotating in the cavity of the C_5Ph_5 group. Thus, we see a powder-like spectrum averaged about the molecular *z* axis. And, sure enough, the low-field feature has shifted upfield; this shift, together with the *g* matrix components in the principal axis system, leads to the angle between the molecular and *g* matrix axis systems, $\beta = 15°$. By itself, this angle means little, but it can be used to evaluate the results of a valence theory calculation. Thus, an extended Hückel MO calculation leads to

$$|\mathrm{SOMO}\rangle = a_1|x^2 - y^2\rangle + a_2|z^2\rangle + a_3|xz\rangle$$

$$|\mathrm{HOMO}\rangle_1 = b_1|x^2 - y^2\rangle + b_2|z^2\rangle + b_3|xz\rangle$$

$$|\mathrm{HOMO}\rangle_2 = c_1|xy\rangle + c_2|yz\rangle$$

$$g_{xx} = g_e + \frac{\zeta_{Cr}(a_1c_2 + \sqrt{3}a_2c_2 + a_3c_1)^2}{E_0 - E_2}$$

$$g_{zz} = g_e + \frac{\zeta_{Cr}(2a_1c_1 + a_3c_2)^2}{E_0 - E_2}$$

$$g_{xz} = -\frac{\zeta_{Cr}(2a_1c_1 + a_3c_2)(a_1c_2 + \sqrt{3}a_2c_2 + a_3c_1)^2}{E_0 - E_2}$$

$$\tan 2\beta = -\frac{2g_{xz}}{g_{zz} - g_{xx}}$$

With the EHMO results, $a_1 = 0.538$, $a_2 = 0.216$, $a_3 = -0.194$, $c_1 = 0.582$, and $c_2 = -0.061$, we obtain $\beta = 14.8°$, in excellent agreement with experiment. It is worth noting that *g* matrix components computed from the EHMO results are in very poor agreement, largely because the MO energies are not accurately estimated by the EHMO method. The angle β, which does not depend on $E_0 - E_2$, is remarkably accurately determined by the EHMO calculations, lending further support for the idea that the shapes of MO's are reasonably well predicted by Hückel-type MO calculations.

Table 3. EPR Parameters for $[(Me_3SiC{\equiv}CCF_3)Co_2(CO)_6]^-$ [a]

$\langle g \rangle$	*g*	$\langle A^{Co} \rangle$	*A*
2.012	2.012, 2.007, 2.017	(−) 25.0	(+) 25.4, (−) 60.8, (−) 39.4

[a] $\beta = \pm 15°$.

6. Binuclear Complexes

Our first experience with noncoincident matrix principal axes was with the binuclear complexes $[(RC{\equiv}CR)Co_2(CO)_6]^-$:[15]

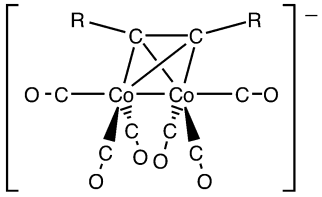

This ion has C_{2v} symmetry, so that the *g* matrix axes must coincide with the molecular axes. However, the Co atoms are not on the 2-fold axis and so must share hyperfine principal axes only in the direction normal to the shared reflection *xz* plane. The symmetry of the problem requires that β, the angle between the g_z axis and the corresponding A_z axis, be equal, but of opposite sign, for the two Co nuclei.

The ramifications of the noncoincidence on the experimental EPR spectrum are rather subtle but became obvious when a serious attempt was made to fit the positions of the spectral features to spin Hamiltonian parameters. The results are summarized in Table 3. EHMO calculations by Hoffmann[16] and chemical evidence[17] suggest that the SOMO is a Co−Co σ^*-orbital, but noncoincidence suggests hybridization:

$$|\mathrm{SOMO}\rangle = a_1(|z^2\rangle_1 - |z^2\rangle_2) + a_2(|xz\rangle_1 + |xz\rangle_2) + \ldots$$

Analysis of the hyperfine interaction leads to $a_1^2 = 0.30$ and $a_2^2 = 0.074$:

$$\tan 2\beta = \frac{2A_{xz}}{A_{zz} - 2A_{xx}} = \pm\frac{2}{\sqrt{3}}\frac{a_2}{a_1}$$

$$\frac{a_2}{a_1} = \frac{1}{2}$$

The SOMO is best described then as an antibonding combination of two Co d_{z^2} orbitals, twisted ±15° away from the *z* axis; in other words, a bent antibonding orbital. Theorists have been talking about bent bonds

(13) Hammack, D. J.; Dillard, M. M.; Castellani, M. P.; Rheingold, A. L.; Rieger, A. L.; Rieger, P. H. *Organometallics* **1996**, *15*, 4791.

(14) Castellani, M. P.; Connelly, N. G.; Pike, R. D.; Rieger, A. L.; Rieger, P. H. *Organometallics* **1997**, *16*, 4369.

(15) Peake, B. M.; Rieger, P. H.; Robinson, B. H.; Simpson, J. *J. Am, Chem. Soc.* **1980**, *102*, 156.

(16) Thorn, D. L.; Hoffmann, R. *Inorg. Chem.* **1978**, *17*, 126.

(17) Arewgoda, M.; Rieger, P. H.; Robinson, B. H.; Simpson, J.; Visco, S. J. *J. Am. Chem. Soc.* **1982**, *104*, 5633.

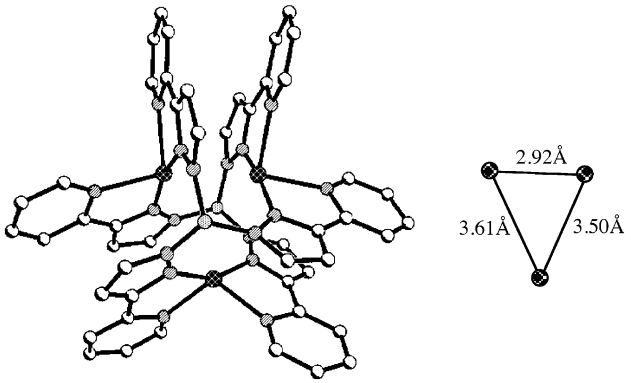

Figure 10. Structure of the Cu(I)−Cu(I)−Cu(I) complex with bridging tris(2-pyridylpyrazolyl)borate ligands.

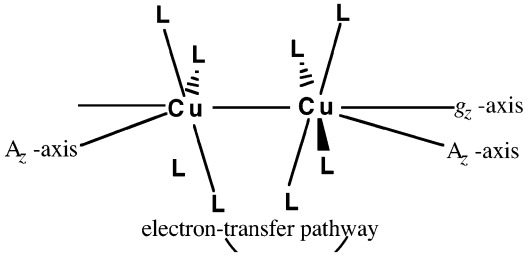

Figure 11. Arrangement of the Cu coordination planes in the low-temperature conformation of the Cu(I)−Cu(I)−Cu(II) complex with bridging tris(2-pyridylpyrazolyl)borate ligands.

for years, but we have actually seen one! Well, at least a bent antibond.

A more recent collaborative project led to a somewhat similar picture. Michael Ward and Jon McCleverty of the University of Bristol have prepared an unusual variation on tris(pyrazolyl)borate by attaching 2-pyridyl groups to each pyrazole, converting the ion into a sexidentate ligand which forms a trinuclear Cu(I) complex, the structure of which is shown in Figure 10.[18] One-electron oxidation results in a Cu(I)−Cu(I)−Cu(II) species which exhibits an isotropic EPR spectrum at 55 °C with hyperfine coupling to one Cu nucleus. However, at temperatures below 120 K, the spectrum (Figure 12) clearly reveals coupling to two equivalent Cu nuclei, but with noncoincident hyperfine matrix axes which recall the Co_2 case discussed above. As the temperature is raised above 120 K, the features of the spectrum broaden and, before the solution melts, a poorly resolved spectrum showing coupling to a single Cu nucleus can be discerned.

Analysis of the two Cu hyperfine structure leads to $\rho_{Cu}^{3d} \approx 0.38$; i.e., 76% of the spin is accounted for by Cu 3d orbitals. The noncoincidence angle $\beta = \pm 16°$ suggests arrangement of Cu coordination planes as shown in Figure 11, as expected if the coordination geometry is little changed from the Cu(I)−Cu(I)−Cu(I) complex (Figure 10). Apparently, rapid electron transfer between two Cu atoms at low temperatures leads to equivalent Cu coupling in the EPR spectrum. However, loss of resolution and high-temperature coupling to one Cu suggests that the odd electron is instantaneously localized on one Cu and that the exchange rate is slow at high temperature (a counterintuitive result!). The explanation must be that molecular motion at high temperatures disrupts the electron-transfer pathway which is most likely via the π-stacking of the pyrazole rings.

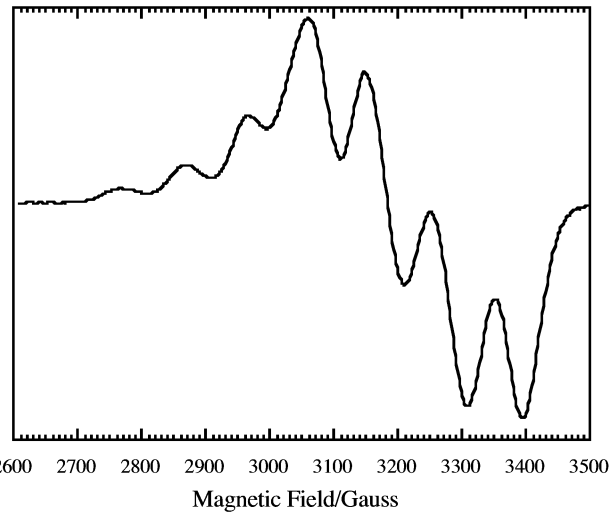

Figure 12. Frozen-solution EPR spectrum of the $[Cu_3]$ complex at 120 K, showing coupling to two equivalent Cu nuclei ($I = {}^3/_2$).

7. Electronic Isomerism

The acetylene-bridged dicobalt anions discussed above readily undergo the nucleophilic displacement reactions[19]

$$[(RC{\equiv}CR)Co_2(CO)_6]^- + CO \rightarrow (RC{\equiv}CR)Co(CO)_3 + [Co(CO)_4]^-$$

$$[(RC{\equiv}CR)Co_2(CO)_6]^- + PR'_3 \rightarrow (RC{\equiv}CR)Co(CO)_2PR'_3 + [Co(CO)_4]^-$$

$$[(RC{\equiv}CR)Co_2(CO)_5PR'_3]^- + PR'_3 \rightarrow (RC{\equiv}CR)Co(CO)(PR'_3)_2 + [Co(CO)_4]^-$$

$$[(RC{\equiv}CR)Co_2(CO)_4(PR'_3)_2]^- + PR'_3 \rightarrow (RC{\equiv}CR)Co(PR'_3)_3 + [Co(CO)_4]^-$$

The resulting mononuclear complexes were characterized by EPR spectroscopy. Isotropic EPR spectra of the mononuclear complexes showed coupling to ^{59}Co and up to three ^{31}P nuclei; since $\langle g \rangle$ and the hyperfine couplings varied slightly with the acetylene substituents, we concluded that these complexes are four-coordinate. Isotropic spectra of the diphosphino complexes showed a line width effect which indicated rapid equilibrium ($\tau \approx 2 \times 10^{-11}$ s at 290 K) between two isomeric forms, apparently one with equivalent ^{31}P nuclei and the other with nonequivalent nuclei. Frozen-solution spectra showed two isomers, with no evidence of noncoincidence of the g and A matrix principal axes.[20] The most obvious

(18) Jones, P. L.; Jeffrey, J. C.; Maher, J. P.; McCleverty, J. A.; Rieger, P. H.; Ward, M. D. *Inorg. Chem.* **1997**, *36*, 3088.

(19) Casagrande, L. V.; Chen, T.; Rieger, P. H.; Robinson, B. H.; Simpson, J.; Visco, S. J. *Inorg. Chem.* **1984**, *23*, 2019.

(20) Casagrande, L. V.; Chen, T.; Rieger, P. H.; Robinson B. H.; Simpson, J.; Visco, S. J. *Inorg. Chem.* **1987**, *22*, 2019. DeGray, J. A.; Meng, Q.; Pieger, P. H. *J. Chem. Soc., Faraday Trans.* **1987**, *83*, 3565.

conclusion, given a four-coordinate d^9 complex, was that these species are square planar with cis and trans isomers (although the rate of the isomerization process seemed unrealistically fast). However, neither the *g* matrix nor the *A* matrix components were consistent with a $d_{x^2-y^2}$ singly occupied orbital, and we were forced to conclude that the complexes are actually tetrahedral with a d_{z^2} SOMO, flying in the face of more than a century of stereochemical tradition that tetrahedral molecules do not have isomeric forms. Our historical conclusions are safe—these are not stereoisomers but electronic isomers which differ only in the orientation of the local *z* axis. Thus, if neither ^{31}P nucleus lies on the *z* axis, they are equivalent, but if one lies on the *z* axis, the nuclei are nonequivalent. The line width effect observed in isotropic spectra then consists simply of the reorientation of the d_{z^2} orbital, expected to be a fast process on the EPR time scale.

OM030565E